

# Co-implantation of Si+N into GaN for *n*-type doping

Yoshitaka Nakano<sup>a)</sup>

*Toyota Central Research and Development Laboratories Inc., Nagakute, Aichi 480-1192, Japan*

Takashi Jimbo

*Nagoya Institute of Technology, Gokiso, Showa, Nagoya 466-8555, Japan*

(Received 30 April 2002; accepted for publication 10 July 2002)

Si-doping characteristics have been systematically investigated for Si+N co-implanted GaN. *n*-type regions were produced in undoped GaN films by the co-implantation and subsequent annealing with an SiO<sub>2</sub> encapsulation layer at high temperatures. The sheet carrier concentration is seen to be precisely controllable between  $3 \times 10^{12}$  and  $5 \times 10^{14}$  cm<sup>-2</sup> with Si activation efficiencies of ~50% when the samples were annealed at 1300 °C. From atomic force microscopic observations, the co-implanted sample shows smooth surface morphology identical to that before implantation, whereas Ga islands are found to be formed in the surface region by the activation annealing in the case of conventional Si implantation. Therefore, the Si+N co-implantation technique turns out to be an effective method to enhance electrical and structural properties in view of GaN stoichiometry. However, implantation-induced microdefects seem to remain even after the high-temperature annealing process for both Si- and Si+N-implanted GaN samples. © 2002 American Institute of Physics. [DOI: 10.1063/1.1504500]

## I. INTRODUCTION

GaN has attracted much interest for high-temperature and high-power electronic devices because of its outstanding properties, such as a wide band gap of 3.39 eV, a high breakdown field of  $5 \times 10^6$  V/cm, and a high saturation drift velocity of  $2.7 \times 10^7$  cm/s.<sup>1,2</sup> Various electronic devices based on GaN-related materials have already been reported.<sup>3-8</sup> Recently, for the design of these electronic devices, especially from a selective-area doping point of view, implantation doping of GaN has become a practical option.<sup>6-12</sup>

In general, group IV and II elements such as Si and Mg are promising donor and acceptor impurities for GaN, respectively. Theory suggests that these elements occupying a Ga-lattice site in GaN will have a low formation energy and will form donor or acceptor energy levels. As for implantation doping of GaN, several *n*- and *p*-type implantation techniques have already been reported with the use of Si<sup>6-12</sup> being the most common dopant for *n*-type and Mg<sup>7-9,13</sup> and Ca,<sup>6,14</sup> the main elements implanted for *p*-type doping. Recent studies have indicated that annealing at high temperatures is effective for high electrical activation of the implanted dopant atoms.<sup>11</sup> However, in the case of conventional implantation, where only one kind of dopant is used, the generation of many N vacancies and self-compensation induced by site switching may occur in the implanted region after the high-temperature annealing process. Therefore, in order to suppress the generation of N vacancies, a N-rich condition should be created prior to implantation of the dopant atoms, and thus the implantation of additional N atoms into GaN might be expected to increase the probability of the particular dopant atoms occupying a Ga-lattice site.<sup>15</sup> In our

previous work,<sup>16</sup> we proposed the co-implantation of N and dopant atoms to achieve high electrical activation of the dopant, and demonstrated that Ge+N co-implantation into GaN can significantly enhance the Ge electrical activation using Ge as an *n*-type dopant for GaN. However, Si-doping characteristics in GaN have not yet been studied by using the co-implantation technique. As mentioned above, Si is the most commonly used dopant which generates *n*-type conductivity in GaN. In addition, the Si implantation is expected to enhance *n*-type electrical activation, because Si is much lighter than Ge and consequently may introduce much less damage in GaN. In this study, we have systematically investigated the Si-doping characteristics of Si+N co-implanted GaN in view of GaN stoichiometry, and the results are compared to those of conventional Si-implanted GaN.

## II. EXPERIMENT

The epitaxial GaN films used in these experiments were 1 μm thick. They were grown on *a*-plane sapphire substrates by metalorganic chemical-vapor deposition at 1050 °C, on a predeposited 20 nm AlN buffer layer grown at 400 °C. The GaN films were not intentionally doped, and showed semi-insulating properties. After growth, the GaN samples were implanted using pure N<sub>2</sub> and SiF<sub>4</sub> gases as the sources of the <sup>14</sup>N and <sup>28</sup>Si species, respectively. First the N<sup>+</sup> ions were implanted at energies of 35, 65, and 100 keV, respectively, to position the ion peak 53, 95, and 143 nm from the surface. The Si<sup>+</sup> ions were then implanted at a fixed energy of 65 keV to place its peak range at the same position as that for the N<sup>+</sup> implanted at 35 keV. The N and Si implant dosages were varied between  $1 \times 10^{13}$  and  $1 \times 10^{16}$  cm<sup>-2</sup>. In the case of the Si+N co-implantation, the N/Si ratio was kept ~1 for an optimum doping.<sup>16</sup> Conventional Si- and N-implanted GaN samples were also prepared for reference. All the im-

<sup>a)</sup> Author to whom correspondence should be addressed; electronic mail: y-nakano@mosk.tytlabs.co.jp

TABLE I. Implant conditions and sample characteristics.

Sample No.	N implant $1 \times 10^{15} \text{ cm}^{-2}$ (keV)	Si implant $1 \times 10^{15} \text{ cm}^{-2}$ (keV)	Sheet carrier concentration ( $10^{14} \text{ cm}^{-2}$ )	Mobility ( $\text{cm}^2/\text{V s}$ )
1	none	65	5.85	80.2
2	35	65	4.87	98.5
3	65	65	5.27	86.8
4	100	65	6.84	75.8

plants were performed at room temperature, with an incidence angle  $7^\circ$  off the normal surface. After implantation, a 500 nm thick  $\text{SiO}_2$  capping layer was deposited on the top surface of the samples by radio-frequency sputtering at room temperature to provide an encapsulation cap for the subsequent implant activation annealing. All the samples were annealed on a SiC-coated graphite susceptor at temperatures between 1100 and 1300  $^\circ\text{C}$  in flowing  $\text{H}_2$  gas at a pressure of 10 Torr. Following the anneal step, HF (49% concentration) was used to remove the  $\text{SiO}_2$  cap, and then Al contacts were formed at the corners of each sample by electron-beam evaporation. Carrier activation was characterized by room-temperature Hall-effect measurements. Hall data of sheet carrier concentration  $n_s$  and electron mobility  $\mu_e$  were in error by less than 1% on these measurements. The depth distribution of the implanted Si atoms was measured by secondary ion mass spectrometry (SIMS). The surface morphology of the implanted region of the GaN samples was analyzed by atomic force microscopy (AFM).

### III. RESULTS AND DISCUSSION

#### A. SIMS profiles of the implanted Si atoms

The dependence of the depth distribution of the implanted Si atoms on the co-implanted N peak range was investigated. The implant conditions for typical samples, numbered 1–4, are summarized in Table I, together with their electrical data. Here, the implanted N and Si dosages were fixed at  $1 \times 10^{15} \text{ cm}^{-2}$ . Figure 1 shows SIMS profiles of the implanted Si atoms before and after annealing at 1300  $^\circ\text{C}$  for 5 min, together with N and Si atomic profiles calculated by Transport of Ions in Matter (TRIM) software. Before the annealing, the experimental peak position of the implanted Si atoms is in reasonable agreement with that of the TRIM calculations, regardless of the implanted N peak range. Furthermore, the implanted Si atoms are found to diffuse into a little deeper-lying region of the GaN films by the annealing at 1300  $^\circ\text{C}$ , which seems to be also independent on the N implant conditions. This annealing-induced diffusion is different from the situation of Ge+N co-implantation.<sup>16</sup> That is, this redistribution of the implanted Si atoms may occur due to Si having much lighter ion mass than Ge. In addition, Si atoms cannot be detected for N-implanted GaN after the annealing by the SIMS measurements. This suggests that the diffusion of Si atoms into GaN from an  $\text{SiO}_2$  encapsulation layer cannot occur during the high-temperature annealing process and consequently that the use of the  $\text{SiO}_2$  cap does not influence the Si-doping characteristics, as discussed later. On the other hand, the diffusion of the implanted N atoms

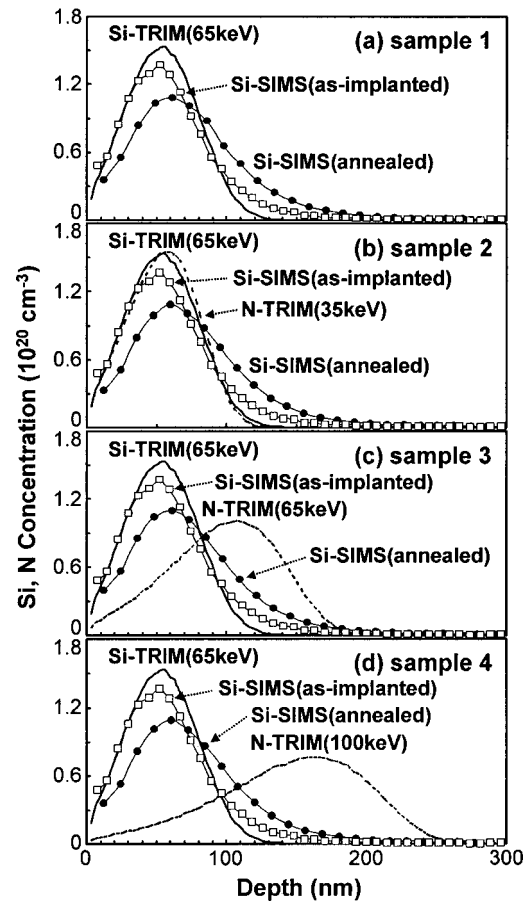


FIG. 1. TRIM simulated atomic profiles of implanted N (dashed line) and Si (solid line) and SIMS profiles of Si implanted in GaN, as-implanted ( $\square$ ) and annealed ( $\bullet$ ) at 1300  $^\circ\text{C}$  for samples 1–4.

cannot be determined because of it being difficult to distinguish the implanted N atoms from the component N atoms of the GaN lattice even when isotope  $^{15}\text{N}$  atoms were implanted.

#### B. Electrical properties

The co-implanted N peak range dependence of the Si activation was investigated for typical samples 1–4. Here, the activation annealing was performed at 1300  $^\circ\text{C}$  for 5 min. First, a different of electrical properties is found between the conventional Si-implanted samples (sample 1) and the Si+N co-implanted sample (sample 2), as shown in Table I. Sample 2 shows a lower  $n_s$  and a higher  $\mu_e$  than sample 1, in spite of the identical Si dosage of  $1 \times 10^{15} \text{ cm}^{-2}$  for both samples. In particular, the high  $\mu_e$  of  $\sim 100 \text{ cm}^2/\text{V s}$  can be achieved even at a Si dosage of  $1 \times 10^{15} \text{ cm}^{-2}$  for the co-implanted sample 2 in which the N peak range is equivalently placed at the Si peak range. This reflects the high quality of the GaN lattice in the co-implanted region compared to the conventional Si-implanted one. Si activation efficiency of sample 2 is estimated to be  $\sim 49\%$  from the implanted Si dosage of  $1 \times 10^{15} \text{ cm}^{-2}$ . As compared to sample, the high  $n_s$  seen for sample 1 may be related to the generation of N vacancies besides the Si electrical activation. That is, there are extremely insufficient N atoms available to maintain GaN sto-

ichiometry in the conventional Si-implanted region. Considering that the N vacancies form a shallow donor level,<sup>17</sup> many carriers can be generated from these N vacancies. As a result, the conventional Si implantation may show an increase in  $n_s$  all the more after introducing the N vacancies. In this case, the concentration of the N vacancies generated should be ideally equal to that of the implanted Si atoms. That is, the effective carriers from the Si doping except for the N vacancies may be assumed to be only half the  $n_s$ . Thus, the actual Si activation efficiency is roughly estimated to be as low as 29% for sample 1, considering the increase in carrier concentration caused by the generation of many N vacancies. On the other hand, in the case of the Si+N co-implanted GaN samples (samples 2–4), the  $n_s$  and  $\mu_e$  strongly depend on the implanted N peak range relative to the Si peak one, as shown in Table I. The  $n_s$  decreases and the  $\mu_e$  increases with close overlapping of the N peak range with the Si peak. From our previous study of the Ge+N co-implantation,<sup>16</sup> the distribution of the co-implanted N atoms is expected to be unchanged even after the annealing at 1300 °C. In addition, the N-implanted GaN sample shows semi-insulating properties after the annealing. Thus, the observed increase in  $n_s$  is considered to be caused by the combined effects of Si doping and N-vacancy generation for the co-implanted samples (samples 3 and 4) in which the N peak range does not completely overlap with the Si peak range. Therefore, we can say that the co-implantation of additional N atoms significantly enhances the actual Si electrical activation when the N peak range is equivalently placed at the Si peak range.

Here, these results on the Si+N co-implantation are compared with our previous study on that of the Ge+N.<sup>16,18</sup> The  $n_s$  and  $\mu_e$  obtained for the Ge+N system are lower than those for the Si+N system, under the same condition where the N peak range overlapped the dopant peak range. In particular, the Ge+N coimplanted GaN samples show much lower  $\mu_e$  of 50–60 cm<sup>2</sup>/V s. In addition, the N peak range dependence of  $n_s$  seen for the Ge+N system is found to be just the opposite of that for the Si+N system. That is, the  $n_s$  increases with relatively low  $\mu_e$  with close overlapping of the N peak range with the Ge peak range for the Ge+N co-implanted GaN samples. These differences that we observed are considered to be caused by a considerable margin of ion mass between Si and Ge; the Ge+N co-implantation process should be inclusive of implantation-induced damage in addition to the combined effects of the Ge-doping and the N-vacancy generation. Conversely, the Si+N co-implantation may suppress the damage due to Si being much lighter than Ge, as expected. Therefore, we can determine that the Si+N co-implantation technique is a more effective method for achieving high quality *n*-type doped GaN by implantation, based on an ideal site-competition effect.

The annealing-condition dependence of the Si activation was also investigated in the Si+N co-implantation process. The implant condition was the same one as sample 2 in which the implanted N peak range overlaps with the Si peak range, as shown in Table I. Figure 2(a) shows room-temperature  $n_s$  and  $\mu_e$  as a function of annealing temperature for the Si+N co-implanted samples. Here, annealing time

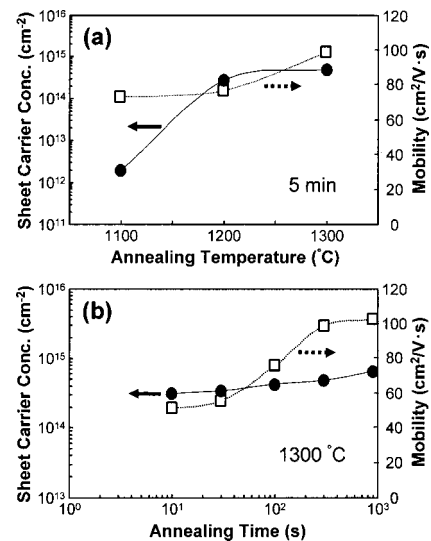


FIG. 2. Sheet carrier concentration (●) and mobility (□) as a function of: (a) annealing temperature and (b) annealing time for Si+N co-implanted GaN samples with Si and N dosages of 1 × 10<sup>15</sup> cm<sup>-2</sup>.

was fixed at 5 min. With the rise of annealing temperature from 1100 to 1200 °C, the  $n_s$  significantly increases from 2 × 10<sup>12</sup> to 3 × 10<sup>14</sup> cm<sup>-2</sup> with high  $\mu_e$  of ~75 cm<sup>2</sup>/V s. This indicates that the Si electrical activation starts to occur at around 1200 °C. On the other hand, the  $\mu_e$  significantly increases in spite of the  $n_s$  being saturated by annealing at 1300 °C. This behavior indicates an improvement in the crystallinity in the electrically activated region. Therefore, annealing at high temperatures above 1200 °C is required to activate the implanted Si atoms in GaN. Figure 2(b) shows room-temperature  $n_s$  and  $\mu_e$  as a function of annealing time at 1300 °C for the Si+N co-implanted samples. The  $n_s$  gradually increases with an increase of annealing time, whereas the  $\mu_e$  significantly increases from 51 to 103 cm<sup>2</sup>/V s. This result also suggests a significant improvement of the crystallinity under an optimum condition of GaN stoichiometry in accordance with increased annealing time.

Moreover, Si-doping characteristics were investigated in view of Si implant dosage. Figure 3 shows the room-temperature  $n_s$  and  $\mu_e$  as a function of Si dosage for the Si+N co-implanted and subsequently annealed GaN samples. Here, the N implantation was performed at 35 keV

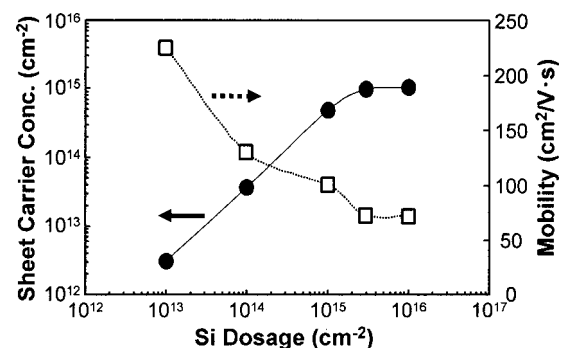


FIG. 3. Sheet carrier concentration (●) and mobility (□) as a function of Si implant dosage for the Si+N co-implanted samples after annealing at 1300 °C.

to overlap the N-implanted region with the Si one as shown in Fig. 1(b), and the N/Si ratio was fixed at 1 for the optimum Si activation as mentioned above. The activation annealing was carried out at 1300 °C for 5 min. The  $n_s$  increases monotonically with increasing Si implant dosage up to  $1 \times 10^{15} \text{ C cm}^{-2}$  under the Si+N co-implantation process, that is, the  $n_s$  seems to be precisely controllable between  $3 \times 10^{12}$  and  $5 \times 10^{14} \text{ C cm}^{-2}$  with respect to the Si dosage. An enhanced Si activation level of  $\sim 50\%$  is attained in this region of the Si dosage. Therefore, improved doping characteristics for Si implantation into GaN can be successfully achieved by the Si+N co-implantation method. On the other hand, the  $\mu_e$  decreases gradually with increasing Si dosage in this region. However, the behavior of the  $\mu_e$  does not seem to be simply consistent with the variation seen for the  $n_s$  in view of ionized impurity scattering. The  $\mu_e$  may be primarily dependent on the combined effect of ionized impurity scattering and space charge scattering induced by the presence of the implantation-introduced defects. In addition, the observed  $\mu_e$  is much higher than results previously reported in the literature. This indicates that the Si+N co-implantation and subsequent annealing might significantly improve the crystallinity of the electrically activated region, which results in suppressing the space charge scattering caused by the generation of defects such as N vacancies as compared with the conventional implantation technique. Furthermore, the  $n_s$  and  $\mu_e$  seem to be saturated at around  $1 \times 10^{15} \text{ cm}^{-2}$  and  $71 \text{ cm}^2/\text{V s}$ , respectively, by increasing the Si dosage above  $3 \times 10^{15} \text{ cm}^{-2}$ . This result suggests that the Si-doping characteristics by the implantation technique may attain the solid-solubility limit of the implanted Si atoms in GaN.

In this study, improved Si-doping characteristics have been achieved for GaN by the Si+N co-implantation where the N/Si ratio was fixed at 1. However, there seem to be numerous implantation-induced damage and N vacancies even after the high-temperature annealing process. Thus, the N/Si ratio needs to be optimized to see improvement in Si-doping characteristics and crystallinity of the co-implanted GaN.

### C. AFM observations

Figures 4(a) and 4(b), respectively, show typical AFM images of the Si-(sample 1) and Si+N-(sample 2) implanted GaN after annealing at 1300 °C for 5 min. A clear difference can be seen between them. In the co-implanted GaN sample, a number of growth steps are clearly observed as shown in Fig. 4(b), whose surface morphology is identical to that of the as-grown GaN before implantation. That is, the surface morphology is found to be unchanged even after the implantation and subsequent annealing processes for the co-implanted GaN. Here, the dark points correspond to threading dislocations. In sharp contrast, many white-colored islands with  $\sim 25 \text{ nm}$  in height and  $\sim 140 \text{ nm}$  in diameter can be seen for the conventional Si-implanted sample, as shown in Fig. 4(a). These islands were found to be composed of Ga from Auger electron spectroscopy (AES) measurements. These Ga islands in the surface region are considered to be

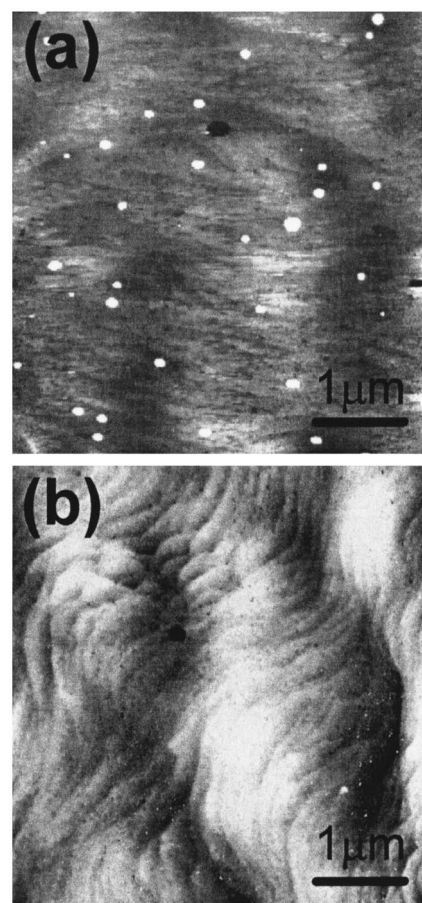


FIG. 4. AFM images of Si- and Si+N-implanted GaN samples with a Si dosage of  $1 \times 10^{15} \text{ cm}^{-2}$  after annealing at 1300 °C. Both images are  $5 \times 5 \mu\text{m}^2$ .

formed in accordance with GaN dissociation caused by the high-temperature annealing. In particular, in the case of the conventional Si implantation, the Ga islands are expected to be more easily formed because there is insufficient N atoms in the implanted region to achieve stoichiometric GaN as compared to the Si+N co-implantation process. In addition, the growth steps are not clearly seen for the Si-implanted sample, which is in reasonable agreement with the GaN dissociation in the surface region. Thus, the Si+N co-implantation turns out to significantly suppress the Ga-island formation in view of GaN stoichiometry. Therefore, we can conclude that the co-implantation technique is more effective in enabling the reconstruction of the GaN lattice in the implanted surface region, resulting in an improvement in the crystallinity of the electrically activated region. However, implantation-induced microdefect “small holes” can be seen even after the high-temperature annealing process for both Si- and Si+N-implanted samples, as shown in Figs. 4(a) and 4(b). For reference, the microdefects cannot be observed for the N-implanted sample after annealing, indicating that the co-implantation of additional N atoms into GaN might be expected to introduce much less damage in the implanted region than the implantation of Si dopant atoms. In addition, the microdefects observed in both the Si- and Si+N-implanted GaN are probably associated with the implantation

of Si atoms and may have some kind of relation to the defects characteristic of both the Ge- and Ge+N-implanted GaN as determined by positron annihilation spectroscopic measurements in our previous study.<sup>18</sup>

#### IV. CONCLUSIONS

We have demonstrated that the Si+N co-implantation into GaN and subsequent annealing at high temperatures can enhance the actual Si electrical activation based on a site-competition effect compared to the conventional Si implantation. In particular, overlapping of the N-implanted region with the Si one makes the Si activation and crystallinity higher. The sheet carrier concentration is found to be precisely controllable between  $3 \times 10^{12}$  and  $5 \times 10^{14} \text{ cm}^{-2}$  with the Si activation efficiencies of  $\sim 50\%$ . From AFM observations, Ga islands are found to be formed in the surface region for the conventional Si-implanted GaN after activation annealing, whereas the island formation is significantly suppressed in the case of the Si+N co-implantation. However, implantation-induced microdefects can be seen to remain even after the high-temperature annealing process for both Si- and Si+N-implanted samples.

#### ACKNOWLEDGMENTS

The authors would like to thank Professor T. Egawa of Nagoya Institute of Technology and Dr. T. Kachi of Toyota

Central Research and Development Laboratories for useful technical discussions.

- <sup>1</sup>H. Morkoc, S. Strite, G. B. Gao, M. E. Lin, B. Sverdlov, and M. Burns, *J. Appl. Phys.* **76**, 1363 (1994).
- <sup>2</sup>T. P. Chow and R. Tyagi, *IEEE Trans. Electron Devices* **41**, 1481 (1994).
- <sup>3</sup>M. Asif. Khan, J. N. Kuznia, A. R. Bhattacharai, and D. T. Olson, *Appl. Phys. Lett.* **62**, 1786 (1993).
- <sup>4</sup>S. C. Binari, L. B. Rowland, W. Kruppa, G. Kelner, K. Doverspike, and D. K. Gaskill, *Electron. Lett.* **30**, 1248 (1994).
- <sup>5</sup>M. Asif. Kahn, A. Bhattacharai, J. N. Kuznia, and D. T. Olson, *Appl. Phys. Lett.* **63**, 1214 (1993).
- <sup>6</sup>J. C. Zolper, R. J. Shul, A. G. Baca, R. G. Wilson, S. J. Pearton, and R. A. Stall, *Appl. Phys. Lett.* **68**, 2273 (1996).
- <sup>7</sup>A. P. Zhang *et al.*, *Appl. Phys. Lett.* **78**, 823 (2001).
- <sup>8</sup>A. P. Zhang *et al.*, *Appl. Phys. Lett.* **76**, 3816 (2000).
- <sup>9</sup>S. J. Pearton, C. B. Vartuli, J. C. Zolper, C. Yuan, and R. A. Stall, *Appl. Phys. Lett.* **67**, 1435 (1995).
- <sup>10</sup>J. C. Zolper, H. H. Tan, J. S. Williams, J. Zou, D. J. H. Cockayne, S. J. Pearton, M. Hagerott Crawford, and R. F. Karlicek, Jr., *Appl. Phys. Lett.* **70**, 2729 (1997).
- <sup>11</sup>X. A. Cao *et al.*, *Appl. Phys. Lett.* **73**, 229 (1998).
- <sup>12</sup>C. J. Eiting, P. A. Grudowski, R. D. Dupuis, H. Hsia, Z. Tang, D. Becher, H. Kuo, G. E. Stillman, and M. Feng, *Appl. Phys. Lett.* **73**, 3875 (1998).
- <sup>13</sup>J. S. Chan *et al.*, *Appl. Phys. Lett.* **68**, 2702 (1996).
- <sup>14</sup>J. C. Zolper, R. G. Wilson, S. J. Pearton, and R. A. Stall, *Appl. Phys. Lett.* **68**, 1945 (1996).
- <sup>15</sup>H. Kobayashi and W. H. Gibson, *Appl. Phys. Lett.* **74**, 2355 (1999).
- <sup>16</sup>Y. Nakano and T. Kachi, *Appl. Phys. Lett.* **79**, 1468 (2001).
- <sup>17</sup>P. Boguslawski, E. L. Briggs, and J. Bernholc, *Phys. Rev. B* **51**, 17255 (1995).
- <sup>18</sup>Y. Nakano and T. Kachi, *J. Appl. Phys.* **91**, 884 (2002).